nature ecology & evolution

Article

https://doi.org/10.1038/s41559-023-02091-z

Low morphological disparity and decelerated rate of limb size evolution close to the origin of birds

Received: 3 February 2023

Accepted: 9 May 2023

Published online: 5 June 2023

Check for updates

Min Wang & Zhonghe Zhou

The origin of birds from theropod dinosaurs involves many changes in musculoskeletal anatomy and epidermal structures, including multiple instances of convergence and homology-related traits that contribute to the refinement of flight capability. Changes in limb sizes and proportions are important for locomotion (for example, the forelimb for bird flight); thus, understanding these patterns is central to investigating the transition from terrestrial to volant theropods. Here we analyse the patterns of morphological disparity and the evolutionary rate of appendicular limbs along avialan stem lineages using phylogenetic comparative approaches. Contrary to the traditional wisdom that an evolutionary innovation like flight would promote and accelerate evolvability, our results show a shift to low disparity and decelerated rate near the origin of avialans that is largely ascribed to the evolutionarily constrained forelimb. These results suggest that natural selection shaped patterns of limb evolution close to the origin of avialans in a way that may reflect the winged forelimb 'blueprint' associated with powered flight.

The assembly of the volant bird body plan from the ancestral bulky dinosaurian condition is an enduring topic of evolutionary biology, encompassing some of the most extensive morphological changes pertaining to powered flight[1–4]. Size miniaturization, forelimb elongation and tail reduction, along with other skeletal modifications, have been hotly discussed, with competing scenarios explaining the modes and patterns of evolutionary origins of the characteristic avialan body plan[4–8]. However, our understanding about the morphological evolution and phylogeny close to the origin of the Avialae and powered flight has been fundamentally refined with newly discovered fossils since those studies. In addition, previous body size-centric analyses may have overlooked local changes[5,6,9–11]; the heterogenous changes within and between the forelimb and hindlimb are essential to decipher clade-specific evolutionary patterns. Therefore, an updated study with larger taxonomic samplings is needed to gain fresh insights into this evolutionary transition and test previous hypotheses. In this study, we used phylogenetic comparative methods to quantify the morphological disparity of limb proportions and estimate the branch-specific and clade-specific evolutionary rate leading to the acquisition of the avialan body plan. This study aimed to address the following questions: How and when did the typical avialan-like limb proportions appear? Did the forelimb and hindlimb respond differently to the selective pressures associated with ecological shifts? Did powered flight as an evolutionary innovation trigger morphological disparity and accelerate evolutionary rate?

Results

Morphological variations

The results of phylogenetic principal component analysis (PCA) using all limb measurements show that non-avialan theropods occupied a larger morphospace than that of early avialans (Fig. 1a,b and Extended Data Fig. 1). This result is robust to different phylogenetic hypotheses (Supplementary Figs. 1–14). Principal component 1 (PC 1) correlates negatively with all limbs with approximately equal eigenvector coefficients (Supplementary Tables 1 and 2), indicating that it describes the overall elongation of limbs (related to body size). PC2 corresponds to the elongation of the forelimb relative to the hindlimb; differences along this axis distinguish avialans from non-paravian theropods, with

Key Laboratory of Vertebrate Evolution and Human Origins, Institute of Vertebrate Paleontology and Paleoanthropology, Chinese Academy of Sciences, Beijing, China. e-mail: wangmin@ivpp.ac.cn

https://doi.org/10.1038/s41559-023-02091-z

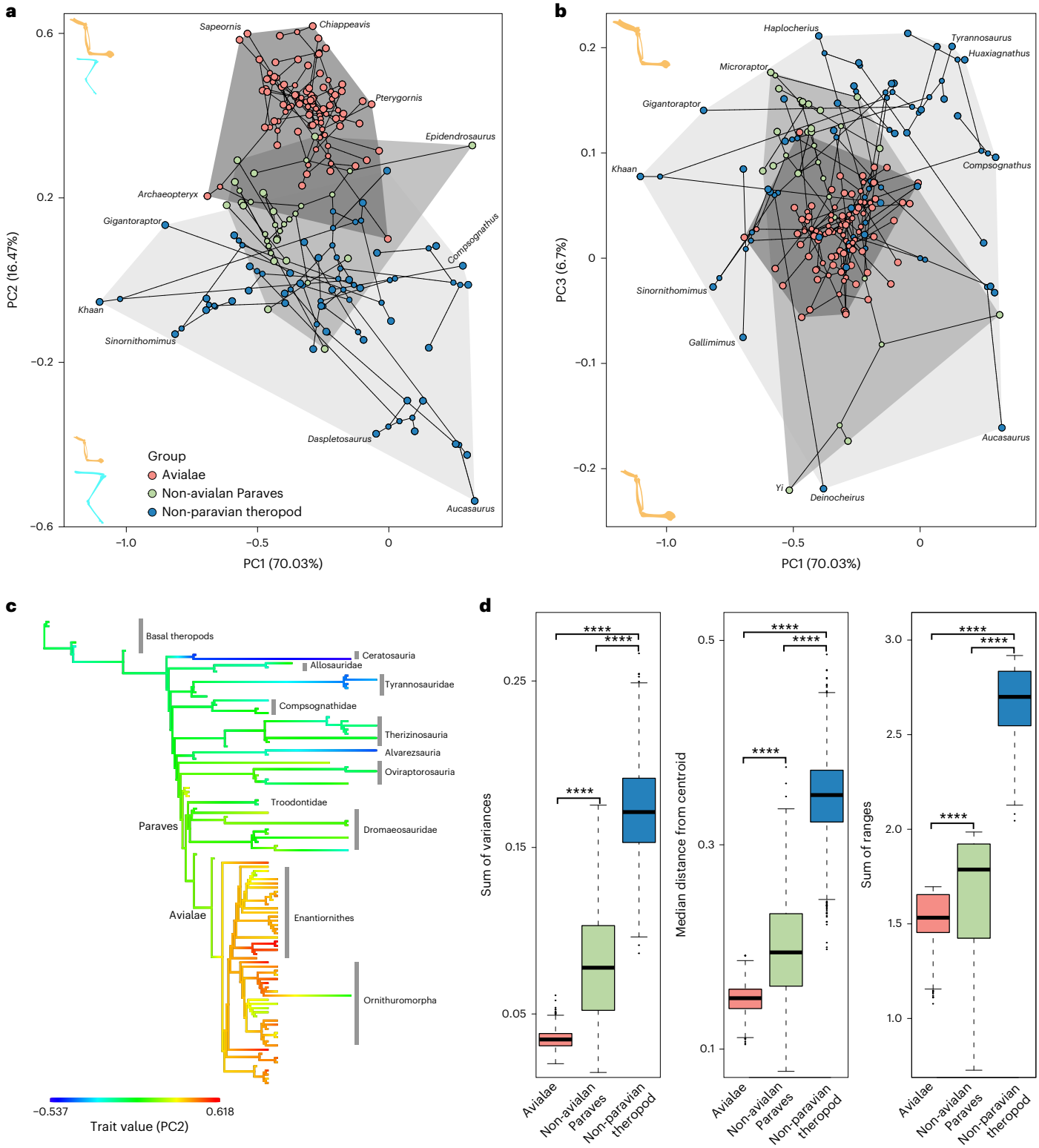

Fig. 1 | Morphological disparity of appendicular elements of Mesozoic theropods. a,**b**, Phylogenetic morphospace of the first three PCs of both forelimb and hindlimb elements (**a**,**b**) (red circles: avialans; green circles: non-avialan paravians; blue circles: non-paravian theropods). **c**, Changes in PC2 across a time-calibrated theropod phylogeny (see Extended Data Fig. 1 for the results of PCs 1 and 3). **d**, Comparison of morphological disparity among subgroups of Mesozoic theropods. (The boxes represent the median and the first and third quartiles of morphological disparity; $n = 109$ species.) Morphological disparity was compared using a Welch's t-test for statistical significance (two-sided ****$P < 0.05$). Taxa placed near the edge of the morphospace are labelled (the results showing the full names of taxa are shown in the figures in the Open Science Framework (OSF)). The interpretative line drawings of the forelimb and hindlimb denote the changes along the principal axes.

non-avialan paravians in the intermediate position. Mapped changes of PC2 across the theropod phylogeny exhibit a clear trend of forelimb elongation along the line to avialans (Fig. 1c), reinforcing the hypothesis that drastic elongation of the forelimb took place close the origin of the Avialae[6,12]. PC3 mainly reflects the elongation of the metacarpal bone relative to the humerus and ulna. Avialans are closely packed and are overwhelmed by the distribution of non-avialan theropods along this axis, attesting to the autapomorphic forelimb configurations seen in scansoriopterygids and alvarezsaurids[12,13]. The permutational multivariate analysis of variance (PERMANOVA) tests show that avialans and non-avialan paravians are statistically separated from each other in morphospace (Supplementary Table 3). Similar patterns were recovered using conventional PCA without accounting for phylogeny and body size (Supplementary Fig. 15 and Supplementary Table 4).

We further analysed the forelimb and hindlimb separately. The results of the phylogenetic PCA of the forelimb showed that PC1 corresponds to the overall size of the forelimb, and that avialans are separated from the larger non-avialan forms (Supplementary Table 5). PC2 describes the elongation of the metacarpal bones relative to the proximal elements. It is worth noting that avialan and non-avialan theropods are clustered along this axis (Fig. 2a and Extended Data Fig. 2), indicating that the proportion of metacarpal bone in the forelimb is constrained, rather than differentiated substantially in response to diverse functional demands among groups (for example, prey capture, flight). However, several non-avialan theropods convergently evolved highly abbreviated metacarpal bones, including scansoriopterygids and ceratosaurs. The short metacarpal in scansoriopterygids may be related to the membranous wing attachment[12]; however, for ceratosaurs it probably reflects reduction given the limited function of the manus[14]. PC3 describes the elongation of the ulna relative to the humerus. Avialans and non-avialan paravians are mixed along this axis, and they are separated from non-paravian theropods (Fig. 2a and Extended Data Fig. 3). The PERMANOVA tests show that avialans and non-avialan paravians are both statistically separated from non-paravian theropods in the forelimb morphospace ($P < 0.05$; Supplementary Table 3).

The results of the phylogenetic PCA of the hindlimb show that avialans, non-avialan paravians and non-paravian theropods overlap substantially in morphospace (Fig. 2b and Extended Data Fig. 3), suggesting that the hindlimb proportions are evolutionarily conservative (contrary to ref. 7). This is somewhat counterintuitive given that the body plan changes substantially (for example, tail reduction and functional decoupling from the hindlimb) and that the locomotion shifts from hip-based in non-avialan theropods to knee-based in early diverging avialans[1,15–17]. The lack of separation in hindlimb morphospace suggests that limb proportion alone cannot explain the functional diversification of the hindlimb among avialan and non-avialan theropods[7]. The PERMANOVA tests recovered statistically significant differences in each pairwise comparisons but not in non-avialan paravians and non-paravian theropods (Supplementary Table 3).

Pattern of morphological disparity

Disparity analyses of all limbs showed that non-paravian theropods, non-avian paravians and avialans are statistically different from one another in all disparity metrics ($P < 0.05$; Supplementary Tables 6–8). Non-paravian theropods are more disparate than non-avian paravians, regardless of the disparity metric choice, whereas early avialans are the least disparate, although contributing more taxa to the dataset (Fig. 1d). The marked discrepancy of disparity among these groups still exists when only the forelimb is analysed, but that gap is greatly diminished when only the hindlimb is investigated (Fig. 2c,d). Rarefaction analyses showed that these results are not strongly affected by sampling bias (Extended Data Fig. 4). Comparable results are obtained using different phylogenetic assumptions (Supplementary Figs. 1–14), as well as conventional PCA (Supplementary Figs. 15–17 and Supplementary Table 9).

Variations of two functional indices

Although limb measurements were size-corrected before the phylogenetic PCA, morphological variations are still dominated by uniform changes of limbs (with PC1 correlating nearly equally with all limbs), suggesting that body size miniaturization, the pronounced change[5,9], deeply shaped the appendicular elements along the stem avialan line. Therefore, local variations that respond directly to diverse ecological and functional demands are presumably shadowed by body size changes. To circumvent this issue, we analysed two size-independent functional morphological indices (brachial index (BI) and crural index (CI)) to investigate the focal changes in the forelimb and hindlimb, respectively (see the Methods for the different calculations of CI for avialan and non-avialan taxa). Avialans are separated from non-avialan theropods in the BI–CI morphospace with phylogeny considered or not, which is most pronounced along the CI axis (Fig. 3a and Extended Data Fig. 5a). Avialans and non-avialan paravians overlap to some degree on the BI axis, and they are spaced from non-paravian theropods, which is consistent with the results using the limb measurements. A notable increase in BI occurs along the branch subtending to the Avialae, but an opposite trend is recovered for the CI (Fig. 3b,c). The results vividly capture how the contrasting locomotion adaptations from cursoriality to powered flight have guided the changes in forelimb and hindlimb. When the CI is calculated as the length ratio between the tibiotarsus and femur for all avialan and non-avialan taxa, avialan taxa are not widely spaced from non-avialan theropods in morphospace (Supplementary Fig. 18).

Avialans are statistically less disparate than non-avialan theropods in the BI and CI, and avialans become more disparate in the CI when this index is calculated the same way across taxa (Extended Data Fig. 5b,c, Supplementary Fig. 9 and Supplementary Table 10). The proportion of wing bones represents a mechanical-level system, whereas BI correlates with different flight modes among extant volant taxa[18,19]. The low variation of the BI among avialans probably reflects strong selection in favour of wing bone proportions optimized for flight. Non-avialan paravians display greater CI variations than other groups; this may have resulted from conflicting and dual demands associated with the use of the hindlimb in locomotion (for example, running and manipulating prey) that is further intensified by their diverse experimentations with volant behaviour (for example, climbing, perching)[7,12,20].

Evolutionary rate

The evolutionary rate of all limbs (PCs 1–4 as the input data) shows a general decreasing trend along the stem avialan line, with derived members of the ornithuromorphs and non-avialan paravians (for example, Oviraptorosauria and Scansoriopterygidae) exhibiting an accelerated rate (Fig. 4a). The results are robust to different phylogenetic hypotheses (Supplementary Figs. 4, 10 and 14). The evolutionary rate is statistically different among avialans, non-avialan paravians and non-paravian theropods (Extended Data Fig. 6a and Supplementary Figs. 4, 10 and 14). The rate of forelimb evolution shows a similar pattern; it exhibits a shift to a lower rate in the Avialae (Fig. 4b). The forelimb of non-avialan paravians evolved significantly faster than that of non-paravian theropods, whereas avialans showed the lowest rate (Extended Data Fig. 6b). Unlike the recovered evolutionary rate of all limbs and forelimbs, no distinct rate shift along the line to avialans was identified in the hindlimb (Fig. 4c). The rate is decreased in later diverging members of the Enantiornithes. In contrast, a previous study found a significantly high evolutionary rate of the hindlimb in avialans compared with non-avialan theropods, and a relatively slower rate in the forelimb[7]. However, the results cannot be directly compared because of different methodologies. For instance, body mass was not accounted for and the evolutionary rate was calculated for individual PC axes[7] rather than analysed together as in this study; also, the larger sample size in the present study may have also impacted the results. Taken together, these results indicate that the distinct rate shift in

https://doi.org/10.1038/s41559-023-02091-z

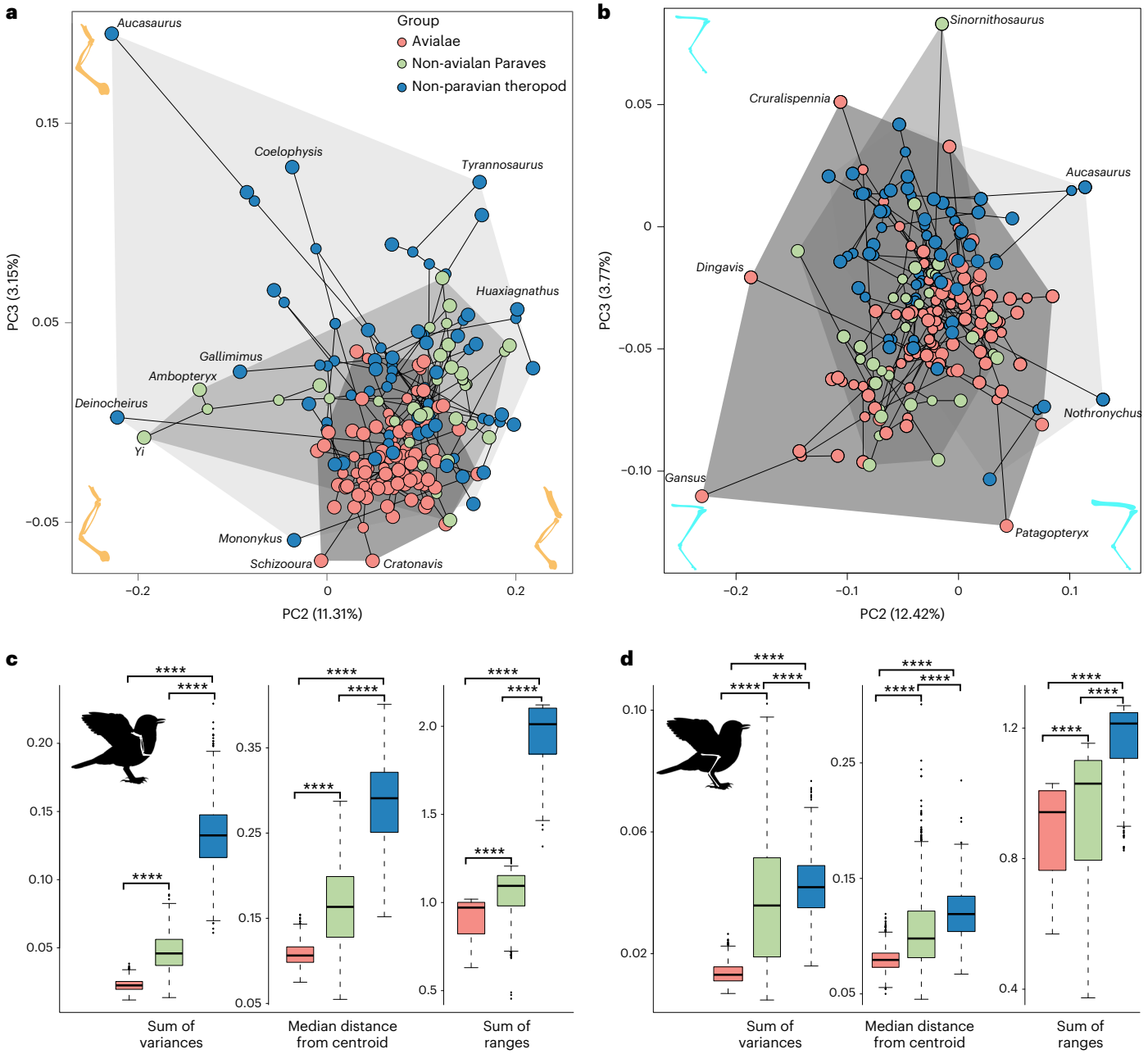

Fig. 2 | Patterns of morphological disparity in the forelimb and hindlimb among Mesozoic theropods. a,**b**, Phylogenetic morphospace of PC2 and PC3 of the forelimb (**a**) and hindlimb (**b**) (see Extended Data Figs. 2 and 3 for additional results). **c**,**d**, Comparison of morphological disparity in the forelimb (**c**) and hindlimb (**d**) among three subgroups of Mesozoic theropods. (The boxes represent the median and the first and third quartiles of morphological disparity; $n = 109$ species.) Morphological disparity was compared using a Welch's t-test for statistical significance (two-sided ****$P < 0.05$). The colour scheme is the same as in Fig. 1. The silhouette has been modified from the diagram created by the Cornell Lab of Ornithology (https://academy.allaboutbirds.org/features/birdanatomy/). Taxa placed near the edge of the morphospace are labelled (the results showing the full names of taxa are shown in the figures in the OSF). The interpretative line drawings of the forelimb and hindlimb denote the changes along the principal axes.

appendicular limb evolution in avialans is largely driven by decelerated forelimb evolution.

The results of the BI analyses showed clade-specific evolutionary rates: accelerated rates seen in basal coelurosaurs and deinonychosaurians; relatively slower rates in other non-avialan theropods; and much slower rates in avialans (Fig. 5a, Extended Data Figs. 7 and 8 and Supplementary Fig. 5). In contrast, the rate of CI evolution showed a different pattern in displaying roughly homogenous rates among non-avialan theropods, although the rate was notably decelerated in avialans (Fig. 5b, Extended Data Figs. 9 and 10 and Supplementary Fig. 6).

Discussion

Our study shows that changes in body plan along the avialan stem lineages are characterized by a decrease in disparity and deceleration in rate of appendicular limb evolution (Figs. 1 and 2, Extended Data Figs. 1–4 and Supplementary Figs. 4–17). This pattern is largely driven by the forelimb, which exhibits constrained morphological variation and slow evolutionary rate close to the origin of the Avialae. With winged forelimbs, the early diverging avialans are separated from non-paravian theropods in morphospace, with non-avialan paravians as intermediates (Fig. 2a, Extended Data Fig. 2 and Supplementary Figs. 1, 7, 11 and 15).

https://doi.org/10.1038/s41559-023-02091-z

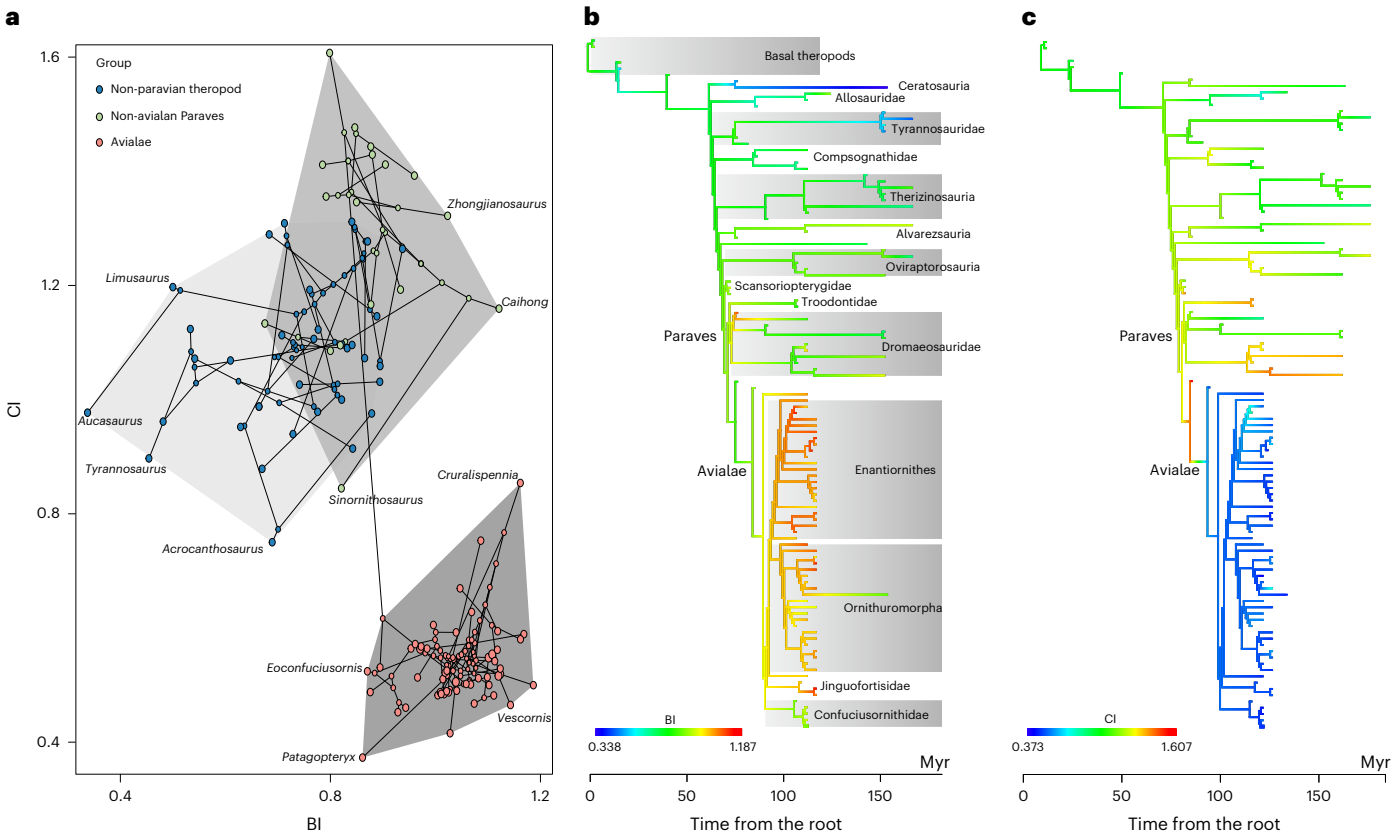

Fig. 3 | Evolutionary changes of two functional indices across the Mesozoic theropod phylogeny. a, Morphospace of BI and CI indices (see Extended Data Fig. 5a for the results that account for the phylogeny). **b**,**c**, Evolutionary changes of the BI (**b**) and CI (**c**). See Extended Data Figs. 7 and 9 for the results with complete taxon labelling. Taxa placed near the edge of the morphospace are labelled (the results showing the full names of taxa are shown in the figures in the OSF). The interpretative line drawings of the forelimb and hindlimb denote the changes along the principal axes.

The extensive forelimb changes and accompanying flight capability would have accelerated the evolutionary rate and increased disparity by opening new niches, a common wisdom regarding adaptative radiation driven by evolutionary novelty[21–23]. However, the opposite pattern was observed in this study. Both the morphological disparity and evolutionary rate of early diverging avialans are statistically significantly lower than those of non-avialan theropods (Figs. 2c and 4b, Extended Data Figs. 4 and 6 and Supplementary Figs. 1, 2, 7, 8, 11, 12, 15 and 16). The longer evolutionary history and presumably the accumulated morphological changes could increase disparity of non-avian theropods but also 'dilute' their evolutionary rate given the increased branch length. For early diverging avialans, that sampling issue may have the opposite effect (lowering disparity and increasing evolutionary rate). Therefore, the recovered low disparity and decelerated rate of morphological evolution of avialans cannot be simply ascribed to sampling bias, and other factors should be considered.

These results also suggest that the forelimb underwent considerable modifications at the cost of its disparity, whereas the hindlimb was evolutionarily conservative well into the diversification of Mesozoic avialans, exhibiting a 'first forelimb and then hindlimb' pattern along the phylogenetic lines towards avialans. The relatively small difference between avialans and non-avialan paravians in disparity and approximation in forelimb morphospace suggest that the bony 'blueprint' of a typical bird wing was formed before the origin of avialans, representing exaptation for flight. Our study complements the results using discrete morphological characters used in previous analyses[24].

The continuously discovered feathered non-avialan theropods suggest that some taxa exhibit morphological modifications related to volant behaviour in parallel to avialan powered flight, such as the hindlimb flight feathers in dromaeosaurids and the membranous wings in scansoriopterygids[12,20,24]. Indeed, we discovered an accelerated evolutionary rate along the branches subtending to these taxa, particularly the scansoriopterygids (Fig. 4 and Supplementary Figs. 1–14). These taxa are also placed near the edge of the morphospace of their group (Figs. 1 and 2), further demonstrating the impact of powered flight on body plan along the stem avialan line.

Comparative analyses of the forelimb show that avialans are distinguishable from other non-avialan theropods in the relative length of the metacarpal and BI (Figs. 2a and 3a and Extended Data Figs. 2 and 5). The proportions of forelimb elements strictly impact the functional performance of avialans, from wing folding when not in use to elaborated movement during flight[3,18,25]. The most obvious condition is that most volant birds have an ulna that is longer than the humerus[18]. This basic bony blueprint required for powered flight probably restricts the morphospace that can be realised by early diverging avialans, resulting in decreased disparity and decelerated evolutionary rate[7]. Although early avialans could fly, derived features that are crucial to refine manoeuvrability in the air are absent in those early members, including pneumaticity of the proximal humerus, a sulcus for guiding flight muscle tendons and quill knobs for attaching secondary remiges[20,26,27]. These and other flight-relevant musculoskeletal features seen in crown groups most probably expand the morphospace by circumventing the constraints of limb proportions, ultimately contributing to the very large forelimb disparity present in extant birds[7,28–30]. The PERMANOVA tests show that avialans and non-avialan paravians are not statistically separated from each other in the forelimb morphospace

https://doi.org/10.1038/s41559-023-02091-z

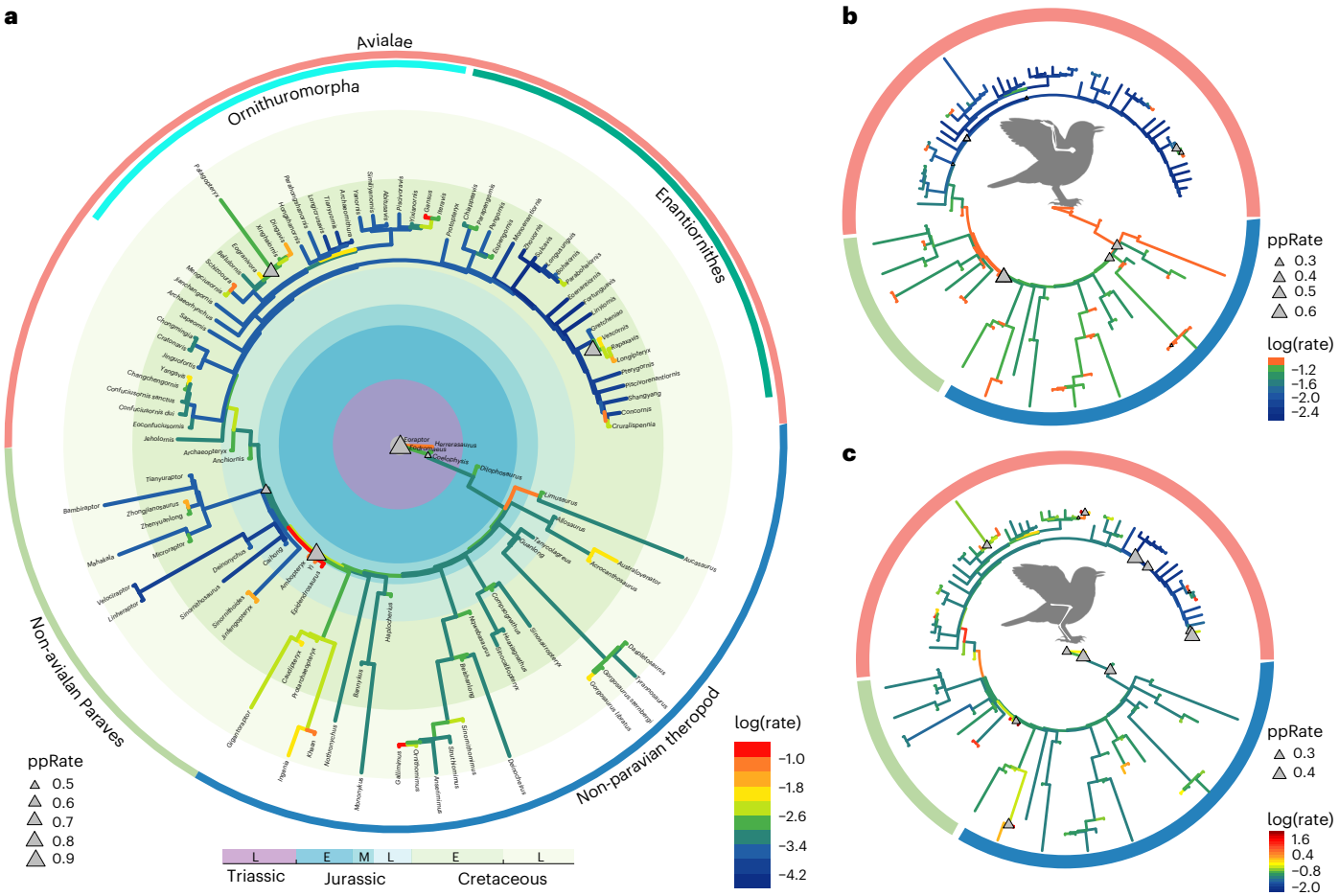

Fig. 4 | Evolutionary rate and rate shift of appendicular elements in Mesozoic theropods. a, All limb elements. **b**, Forelimb. **c**, Hindlimb. Branch-specific evolutionary rates are denoted by the colour gradients. The posterior probabilities of rate shifts are indicated by the relative size of the grey triangles. The silhouette was modified from the diagram created by the Cornell Lab of Ornithology. E, early; L, late; M, middle; ppRate, posterior probability of rate shift.

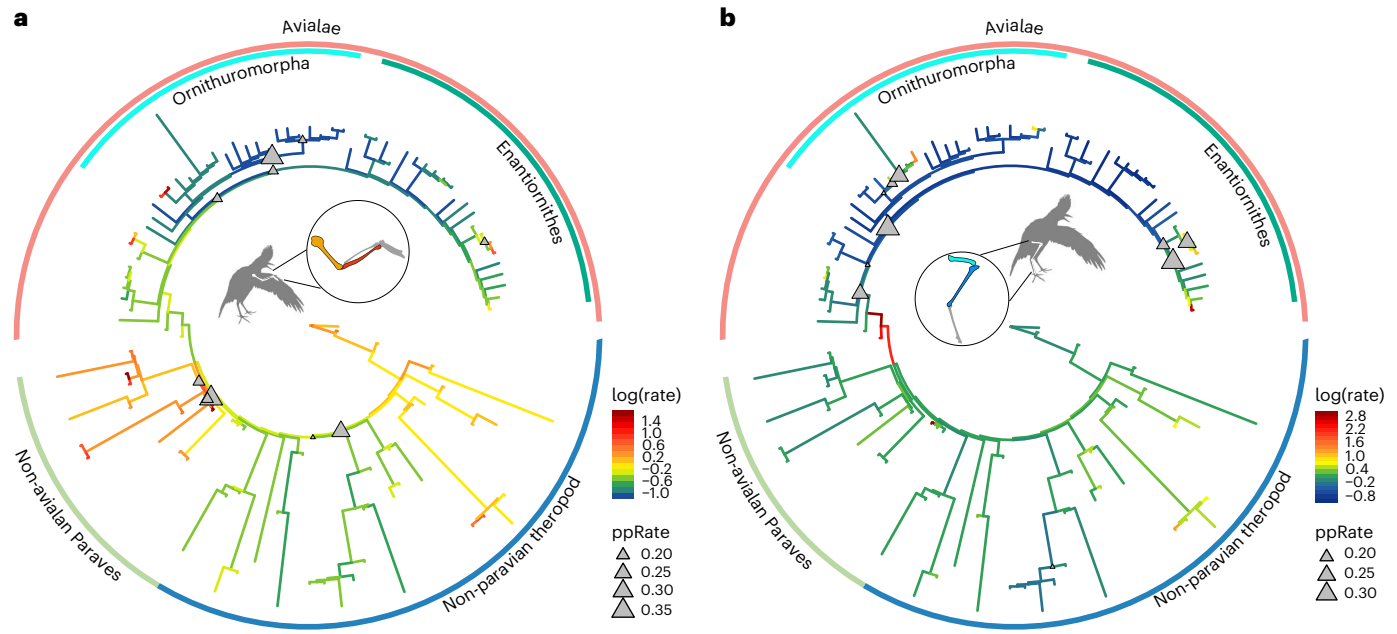

Fig. 5 | Evolutionary rate and rate shift of BI and CI across the Mesozoic theropod phylogeny. a, BI. **b**, CI. See Extended Data Figs. 8 and 10 for the results with the complete names of taxa. Branch-specific evolutionary rates are denoted by the colour gradients. The posterior probabilities of rate shifts are indicated by the relative size of the grey triangles.

but they are both statistically separated from non-paravian theropods in the forelimb morphospace. For the hindlimb, statistically significant separations, found in each pairwise comparison but not non-avialan paravians and non-paravian theropods, suggest that the avialan-like limb proportions were established earlier in the forelimb than in the hindlimb in theropod history, supporting the 'pectoral early–pelvic late' hypothesis[31–33]. Taken together, the recovered patterns of disparity and rate of appendicular limb evolution demonstrate how the early avialan body plan has been shaped deeply by natural selection driven by powered flight.

Methods

Taxonomic sampling and morphological traits

To investigate changes in body shape close to the origin of the Avialae, we compiled linear measurements of limb bones across the whole spectrum of the Mesozoic theropod phylogeny, including early diverging avialans. The length measurements—humerus, ulna and radius, metacarpal II (carpometacarpus bone for avialans), femur, tibia (tibiotarsus for avialans) and metatarsal III (tarsometatarsus bone for avialans)—were obtained by direct measurement combined with published source data (Supplementary Table 1). These limb bones were chosen because they are generally well preserved and are often reported in studies, making it feasible to trace their changes over large temporal and phylogenetic scales. In addition, they have been frequently used to infer the ecology of animals (particularly fossil taxa) because of their functional and ecological relevance[15,17,28,30,34]. We omitted specimens that did not preserve complete length for all six limb bones, given the controversy regarding scaling relationships of limb size. All sampled specimens were sub-adults or adults based on the well-ossified periosteal surface of preserved elements, fusion degree of compound bones and bone histology whenever this information was available. The dataset consisted of 109 taxa (avialans $n = 55$, non-avialan paravians $n = 17$, non-paravian theropods $n = 37$), encompassing nearly all well-recognized taxa, particularly those lineages that are phylogenetically close to the origins of powered flight and avialans. To our knowledge, it represents the most comprehensive dataset of this kind that focuses on limb bone changes across the non-avialan theropod–bird transition, for example, 92 taxa (including 8 invalid taxa) that had six complete limb bones in ref. 7 and 39 taxa in ref. 8.

Phylogenetic inference

Although our understanding about the interrelationships between non-avialan theropods and early diverging avialans, respectively, has been advanced by recent studies[20,26,35–37], a unified study explicitly focusing on this broad phylogeny with sufficient taxonomic representations is lacking. Therefore, an informal supertree was assembled using combined information from recent phylogenetic studies of avialan and non-avialan theropods[13,35,37–39]. To account for taxa with competing phylogenetic placements in different hypotheses, especially taxa close to the origin of avialans whose phylogenetic positions have long been debated, such as *Anchiornis* and the scansoriopterygids: *Anchiornis* was assigned to avialans or troodontids[2,20,24,35] and scansoriopterygids were considered as a sister clade uniting avialans and deinonychus, or as sister clade to oviraptorans[12,35,40]. Given that these taxa are close to the node of the Avialae (the focus of this study), we manually assembled four informal supertrees that explicitly account for the uncertainty of those taxa. Specifically, supertree I treats *Anchiornis* as avialan and the scansoriopterygids as a sister clade that units avialan, troodontids and dromaeosaurids; supertree II treats *Anchiornis* as troodontids and scansoriopterygids as in supertree I; supertree III treats *Anchiornis* as avialan and scansoriopterygids as a sister clade to oviraptorans; and super tree IV treats *Anchiornis* as troodontid and scansoriopterygids as in supertree IV. As for other taxa with competing phylogenetic positions among studies, branches subtending to these taxa were collapsed as polytomies. Our main conclusions are not strongly impacted by phylogenetic assumptions; thus, only the results derived from supertree I is described in the main text (see the Supplementary Information for results derived from other phylogenies). Because the downstream comparative analyses methodologically require fully resolved trees, polytomies were randomly resolved using the multi2di function in the R package ape[41]. To account for phylogenetic uncertainty, the four primary supertrees were each randomly resolved 20 times, resulting in 80 phylogenetic trees that were subjected to the following analyses. The fully resolved supertree was time-calibrated using tip dates bracketed by the first and last appearance datum of the geological stages or epochs in which a given taxon was collected. We applied both the 'minimum branch length' (mbl; here, one million years) and 'equal' methods to calibrate the tree using the timePaleoPhy function in the R package paleotree[42]. The dated supertree was fed into subsequent comparative analyses as the phylogenetic backbone (Extended Data Figs. 1–10 and Supplementary Figs. 1–23; see other results at the OSF). The different tree-calibrating methods did not alter our conclusion; thus, the results from the mbl method are reported in the main text (results derived from the 'equal' method are available at the OSF). Other time-calibrating methods are available that have now being applied to palaeontology, such as cal3 method and the fossilized birth–death model within a Bayesian framework[43–46]. However, these sophisticated methods may not be applicable to our dataset and discrete morphological characters because they require previous parameters (for example, sampling estimates, origination and extinction rates) that are only available for groups whose taxa have a true temporal range[47,48], whereas most of the known Mesozoic theropods including avialans are known from either a single specimen or a limited geological area.

Patterns of morphological disparity

To quantify and compare morphological variation along the line to early diverging avialans, we used phylogenetic PCA to explore patterns and modes of limb proportion evolution among taxa included in the dataset. Traditional PCA analyses (without accounting for phylogeny and body mass) were also performed for comparison. The length measurements were log-transformed before the analyses to normalize the distribution[49]. The species included exhibited approximately 100-fold size differences; thus, we performed a phylogenetic generalized square regression of the log-transformed limb data against body mass using the phyl.resid function in the R package phytools to account for the size-dependent limb measurements[50–52]. Body mass was estimated using an empirical equation derived from living bipedal tetrapods[9,53], which is based on the mediolateral/anteroposterior width of the femoral shaft[9]. The resulting size-corrected length residues were subjected to phylogenetic PCA to account for non-independence in trait values between species because of shared history[54] using the phyl.pca function in the R package phytools[51]. Phylogenetic PCA was applied to forelimb and hindlimb together and separately to analyse changes in the whole body and focal regions that potentially exhibit different patterns in response to major shifts in locomotion and habitats (for example, cursoriality, flight, arboreal species) (Supplementary Tables 2, 4 and 5). To visualize the evolutionary path of limb proportion towards early branching avialans, a phylogenetic morphospace was constructed using PCs.

We quantified and compared the disparity in limb proportion among major groups by assessing each specie's PC scores. Three widely used disparity matrices were calculated: the sum of ranges and variances, and the median distance from centroids[55,56]. Ranges describe the distribution of morphological changes in sampled species and are relatively free from the bias caused by the splitting of specimens. Variances capture the average dissimilarity among specimens and thus are relatively independent from sample size bias[56]. The median distance from centroids captures the median Euclidean distance of individual specimens from the centroid or their group in morphospace occupation[55]. For intergroup comparisons, we subdivided taxa into three major

groups: Avialae; non-avialan Paraves; and non-paravian theropods. The Avialae were further divided into non-ornithothoracine Avialae, Enantiornithes and Ornithuromorpha. Given the uneven species numbers among these groups, rarefaction analyses were performed to determine to what extent morphological disparity is affected by sampling bias. The disparity analyses were performed using the R package disRity[57]. A Welch's *t*-test was used to test whether the disparity matrices were statistically different among major groups using the test.dispRity function in the R package disRity[57]. To test whether some groups were statistically distinct from other groups in morphospace occupation, a non-parametric multivariate analysis of variance (PERMANOVA) test was performed using the adonis function of the R package vegan (Supplementary Tables 3 and 9)[58].

Quantitative functional indices

In addition to limb measurements, two commonly used functional indices were analysed: the BI and CI. The BI (ulna and humerus length) provides an accurate and reliable way of predicting external wing morphology, and thus correlates with different flight models in crown birds[18,19,59]. This ratio is less than 1.0 in most flightless birds and non-avialan theropods[17]. Few attempts have been made to quantify its changes across the theropod phylogeny, particularly near the origin of powered flight. The CI is widely used to assess the terrestrial locomotion performance of tetrapods (for example, speed, stride) and other aspects of ecological adaptations, such as prey capture and stability during perching[34,60,61]. For non-avialan theropods, the CI is calculated as the length ratio between the tibia and femur, whereas for avialans, it is calculated as the length ratio between the tarsometatarsus and tibiotarsus because of the nearly horizontally oriented femur and knee-based locomotion in avialans[16,17]. We also calculated the CI as the length ratio between the tibia and femur for all avialan and non-avialan theropods for comparison. The two indices, which are size-independent, were fed into comparative analyses to explore their evolutionary changes and intergroup disparity comparisons, following the same steps outlined above.

Rates of morphological evolution

We quantified the evolutionary rate of limb proportion across the phylogeny within a Bayesian framework using the BayesTraits v.4 tool (http://www.evolution.reading.ac.uk/BayesTraitsV4.0.1/BayesTraitsV4.0.1.html). PC scores from the PC axes that account for more than 95% of the variances were used as the input data for all limbs, forelimb and hindlimb analyses, respectively. For the BI and CI analyses, raw values were used. We applied a variable rate model and reversible-jump Markov chain Monte Carlo method to estimate branch-specific and clade-specific evolutionary rates, as well as the location, probability and magnitude of rate shifts. Two independent runs were performed, each with 100 million generations for limb data and 50 million generations for CI and BI, respectively (to get convergence and a >200 effective sample size). The first 25% of samples were discarded as burn-in; every 1,000 generations were sampled. A stepping stone sampler algorithm was used to estimate marginal likelihood, with a setting of 500 stones for every 5,000 generations. Chain convergence and effective sample size were determined using the gelman.diag and effectiveSize functions in the R package coda (Supplementary Figs. 19–23 and Supplementary Table 11)[62]. The branch-specific evolutionary rate and posterior probability of rate shift from BayesTraits v.4 were extracted using the R package btrtools (https://github.com/hferg/BTRTools). The average evolutionary rate was plotted across the tree using the protocol outlined in ref. 63. The evolutionary rates among subdivided groups were compared using a mean rate scalar followed by a non-parametric *t*-test for statistical significance.

Reporting summary

Further information on research design is available in the Nature Portfolio Reporting Summary linked to this article.

Data availability

Supplementary material is available online. The R code, raw data and results derived from the phylogeny scaled using the 'equal' method, and the different phylogenetic hypotheses are available on the OSF (https://osf.io/8n3wt/?view_only=753148d6a15f478e8fa027890b6b9bde).

Code availability

The R code used in the comparative analyses is archived and available on the OSF (https://osf.io/8n3wt/?view_only=753148d6a15f478e8fa027890b6b9bde).

References

1. Brusatte, S. L., O'Connor, J. K. & Jarvis, E. D. The origin and diversification of birds. *Curr. Biol.* **25**, R888–R898 (2015).
2. Xu, X. et al. An integrative approach to understanding bird origins. *Science* **346**, 1253293 (2014).
3. Middleton, K. M. & Gatesy, S. M. Theropod forelimb design and evolution. *Zool. J. Linn. Soc.* **128**, 149–187 (2000).
4. Gatesy, S. M. & Dial, K. P. Locomotor modules and the evolution of avian flight. *Evolution* **50**, 331–340 (1996).
5. Lee, M. S. Y., Cau, A., Naish, D. & Dyke, G. J. Sustained miniaturization and anatomical innovation in the dinosaurian ancestors of birds. *Science* **345**, 562–566 (2014).
6. Dececchi, T. A. & Larsson, H. C. E. Body and limb size dissociation at the origin of birds: uncoupling allometric constraints across a macroevolutionary transition. *Evolution* **67**, 2741–2752 (2013).
7. Benson, R. B. J. & Choiniere, J. N. Rates of dinosaur limb evolution provide evidence for exceptional radiation in Mesozoic birds. *Proc. Biol. Sci.* **280**, 20131780 (2013).
8. Hedrick, B. P., Manning, P. L., Lynch, E. R., Cordero, S. A. & Dodson, P. The geometry of taking flight: limb morphometrics in Mesozoic theropods. *J. Morphol.* **276**, 152–166 (2015).
9. Benson, R. B. J. et al. Rates of dinosaur body mass evolution indicate 170 million years of sustained ecological innovation on the avian stem lineage. *PLoS Biol.* **12**, e1001853 (2014).
10. Hone, D. W. E., Dyke, G. J., Haden, M. & Benton, M. J. Body size evolution in Mesozoic birds. *J. Evol. Biol.* **21**, 618–624 (2008).
11. Butler, R. J. & Goswami, A. Body size evolution in Mesozoic birds: little evidence for Cope's rule. *J. Evol. Biol.* **21**, 1673–1682 (2008).
12. Wang, M., O'Connor, J. K., Xu, X. & Zhou, Z. A new Jurassic scansoriopterygid and the loss of membranous wings in theropod dinosaurs. *Nature* **569**, 256–259 (2019).
13. Xu, X. et al. Two Early Cretaceous fossils document transitional stages in alvarezsaurian dinosaur evolution. *Curr. Biol.* **28**, 2853–2860 (2018).
14. Ruiz, J., Torices, A., Serrano, H. & López, V. The hand structure of *Carnotaurus sastrei* (Theropoda, Abelisauridae): implications for hand diversity and evolution in abelisaurids. *Palaeontology* **54**, 1271–1277 (2011).
15. Gatesy, S. M. Hind limb scaling in birds and other theropods: implications for terrestrial locomotion. *J. Morphol.* **209**, 83–96 (1991).
16. Allen, V. R., Kilbourne, B. M. & Hutchinson, J. R. The evolution of pelvic limb muscle moment arms in bird-line archosaurs. *Sci. Adv.* **7**, eabe2778 (2021).
17. Dececchi, T. A. & Larsson, H. C. E. Assessing arboreal adaptations of bird antecedents: testing the ecological setting of the origin of the avian flight stroke. *PLoS ONE* **6**, e22292 (2011).
18. Nudds, R. L., Dyke, G. J. & Rayner, J. M. V. Avian brachial index and wing kinematics: putting movement back into bones. *J. Zool.* **272**, 218–226 (2007).
19. Wang, X. & Clarke, J. A. Phylogeny and forelimb disparity in waterbirds. *Evolution* **68**, 2847–2860 (2014).
20. Pei, R. et al. Potential for powered flight neared by most close avialan relatives, but few crossed its thresholds. *Curr. Biol.* **30**, 4033–4046 (2020).

21. Cooney, C. R. et al. Mega-evolutionary dynamics of the adaptive radiation of birds. *Nature* **542**, 344–347 (2017).
22. Erwin, D. H. Novelty and innovation in the history of life. *Curr. Biol.* **25**, R930–R940 (2015).
23. Sullivan, C., Xu, X. & O'Connor, J. K. Complexities and novelties in the early evolution of avian flight, as seen in the Mesozoic Yanliao and Jehol Biotas of Northeast China. *Palaeoworld* **26**, 212–229 (2017).
24. Brusatte, S. L., Lloyd, G. T., Wang, S. C. & Norell, M. A. Gradual assembly of avian body plan culminated in rapid rates of evolution across the dinosaur-bird transition. *Curr. Biol.* **24**, 2386–2392 (2014).
25. Sullivan, C., Hone, D. W. E., Xu, X. & Zhang, F. The asymmetry of the carpal joint and the evolution of wing folding in maniraptoran theropod dinosaurs. *Proc. Biol. Sci.* **277**, 2027–2033 (2010).
26. Wang, M. & Zhou, Z. in *The Biology of the Avian Respiratory System* (ed. Maina N. J.) 1–26 (Springer International Publishing, 2017).
27. Chiappe, L. M. & Walker, C. A. in *Mesozoic Birds: Above the Heads of Dinosaurs* (eds Chiappe, L. M. & Witmer, L. M.) 240–267 (Univ. California Press, 2002).
28. Tobias, J. A. et al. AVONET: morphological, ecological and geographical data for all birds. *Ecol. Lett.* **25**, 581–597 (2022).
29. Dyke, G. J. & Nudds, R. L. The fossil record and limb disparity of enantiornithines, the dominant flying birds of the Cretaceous. *Lethaia* **42**, 248–254 (2009).
30. Pigot, A. L. et al. Macroevolutionary convergence connects morphological form to ecological function in birds. *Nat. Ecol. Evol.* **4**, 230–239 (2020).
31. Wang, M. & Lloyd, G. T. Rates of morphological evolution are heterogeneous in Early Cretaceous birds. *Proc. Biol. Sci.* **283**, 20160214 (2016).
32. Zhang, C. & Wang, M. Bayesian tip dating reveals heterogeneous morphological clocks in Mesozoic birds. *R. Soc. Open Sci.* **6**, 182062 (2019).
33. Chiappe, L. M. The first 85 million years of avian evolution. *Nature* **378**, 349–355 (1995).
34. Gatesy, S. M. & Middleton, K. M. Bipedalism, flight, and the evolution of theropod locomotor diversity. *J. Vertebr. Paleontol.* **17**, 308–329 (1997).
35. Turner, A. H., Makovicky, P. J. & Norell, M. A. A review of dromaeosaurid systematics and paravian phylogeny. *Bull. Am. Mus. Nat. Hist.* **371**, 1–206 (2012).
36. Pol, D. & Goloboff, P. A. The impact of unstable taxa in coelurosaurian phylogeny and resampling support measures for parsimony analyses. *Bull. Am. Mus. Nat. Hist.* **440**, 97–115 (2020).
37. Wang, M., Lloyd, G. T., Zhang, C. & Zhou, Z. The patterns and modes of the evolution of disparity in Mesozoic birds. *Proc. Biol. Sci.* **288**, 20203105 (2021).
38. Lee, Y.-N. et al. Resolving the long-standing enigmas of a giant ornithomimosaur *Deinocheirus mirificus*. *Nature* **515**, 257–260 (2014).
39. Rauhut, O. W. M. & Pol, D. Probable basal allosauroid from the early Middle Jurassic Cañadón Asfalto Formation of Argentina highlights phylogenetic uncertainty in tetanuran theropod dinosaurs. *Sci. Rep.* **9**, 18826 (2019).
40. O'Connor, J. K. & Sullivan, C. Reinterpretation of the Early Cretaceous maniraptoran (Dinosauria: Theropoda) *Zhongornis haoae* as a scansoriopterygid-like non-avian, and morphological resemblances between scansoriopterygids and basal oviraptorosaurs. *Vertebr. PalAsiat.* **52**, 3–30 (2014).
41. Paradis, E., Claude, J. & Strimmer, K. APE: analyses of phylogenetics and evolution in R language. *Bioinformatics* **20**, 289–290 (2004).
42. Bapst, D. W. paleotree: an R package for paleontological and phylogenetic analyses of evolution. *Methods Ecol. Evol.* **3**, 803–807 (2012).
43. Stadler, T. Sampling-through-time in birth–death trees. *J. Theor. Biol.* **267**, 396–404 (2010).
44. Bapst, D. W. A stochastic rate-calibrated method for time-scaling phylogenies of fossil taxa. *Methods Ecol. Evol.* **4**, 724–733 (2013).
45. Ballell, A., Moon, B. C., Porro, L. B., Benton, M. J. & Rayfield, E. J. Convergence and functional evolution of longirostry in crocodylomorphs. *Palaeontology* **62**, 867–887 (2019).
46. Herrera-Flores, J. A., Stubbs, T. L. & Benton, M. J. Ecomorphological diversification of squamates in the Cretaceous. *R. Soc. Open Sci.* **8**, 201961 (2021).
47. Gavryushkina, A. & Zhang, C. in *The Molecular Evolutionary Clock: Theory and Practice* (ed. Ho, S. Y. W.) 175–193 (Springer, 2020).
48. Wright, A. M., Bapst, D. W., Barido-Sottani, J. & Warnock, R. C. M. Integrating fossil observations into phylogenetics using the fossilized birth–death model. *Annu. Rev. Ecol. Evol. Syst.* **53**, 251–273 (2022).
49. Benson, R. B. J., Godoy, P., Bronzati, M., Butler, R. J. & Gearty, W. Reconstructed evolutionary patterns for crocodile-line archosaurs demonstrate impact of failure to log-transform body size data. *Commun. Biol.* **5**, 171 (2022).
50. Revell, L. J. Size-correction and principal components for interspecific comparative studies. *Evolution* **63**, 3258–3268 (2009).
51. Revell, L. J. phytools: an R package for phylogenetic comparative biology (and other things). *Methods Ecol. Evol.* **3**, 217–223 (2012).
52. Grafen, A. The phylogenetic regression. *Philos. Trans. R. Soc. Lond. B Biol. Sci.* **326**, 119–157 (1989).
53. Campione, N. E. & Evans, D. C. A universal scaling relationship between body mass and proximal limb bone dimensions in quadrupedal terrestrial tetrapods. *BMC Biol.* **10**, 60 (2012).
54. Felsenstein, J. Phylogenies and the comparative method. *Am. Nat.* **125**, 1–15 (1985).
55. Wills, M. A., Briggs, D. E. G. & Fortey, R. A. Disparity as an evolutionary index: a comparison of Cambrian and recent arthropods. *Paleobiology* **20**, 93–130 (1994).
56. Foote, M. Morphological and taxonomic diversity in a clade's history: the blastoid record and stochastic simulations. *Contrib. Mus. Paleontol. Univ. Mich.* **28**, 101–140 (1991).
57. Guillerme, T. dispRity: a modular R package for measuring disparity. *Methods Ecol. Evol.* **9**, 1755–1763 (2018).
58. Oksanen, J. et al. Package 'vegan'. Community Ecology Package. R package version 2.6-2 https://cran.r-project.org/web/packages/vegan/vegan.pdf (2007).
59. Nudds, R. L., Dyke, G. J. & Rayner, J. M. V. Forelimb proportions and the evolutionary radiation of Neornithes. *Proc. Biol. Sci.* **271**, S324–S327 (2004).
60. Samuels, J. X. & Van Valkenburgh, B. Skeletal indicators of locomotor adaptations in living and extinct rodents. *J. Morphol.* **269**, 1387–1411 (2008).
61. Zeffer, A., Johansson, L. C. & Marmebro, Å. Functional correlation between habitat use and leg morphology in birds (Aves). *Biol. J. Linn. Soc. Lond.* **79**, 461–484 (2003).
62. Plummer, M., Best, N., Cowles, K. & Vines, K. CODA: convergence diagnosis and output analysis for MCMC. *R. News* **6**, 7–11 (2006).
63. Felice, R. N. et al. Decelerated dinosaur skull evolution with the origin of birds. *PLoS Biol.* **18**, e3000801 (2020).

Acknowledgements
We thank R. N. Felice for help in calculating the evolutionary rates in R. This research is supported by the National Natural Science Foundation of China (nos. 42225201 and 42288201), the Key Research Program of Frontier Sciences, the Chinese Academy of Sciences (no. ZDBS-LY-DQC002) and the Tencent Foundation (through the XPLORER PRIZE).

Author contributions
M.W. conceived the project. M.W. and Z.Z. performed the analyses and wrote the manuscript.

Competing interests
The authors declare no competing interests.

Additional information
Extended data is available for this paper at https://doi.org/10.1038/s41559-023-02091-z.

Supplementary information The online version contains supplementary material available at https://doi.org/10.1038/s41559-023-02091-z.

Correspondence and requests for materials should be addressed to Min Wang.

Peer review information *Nature Ecology & Evolution* thanks Stephen Brusatte and Gregory Funston for their contribution to the peer review of this work.

https://doi.org/10.1038/s41559-023-02091-z

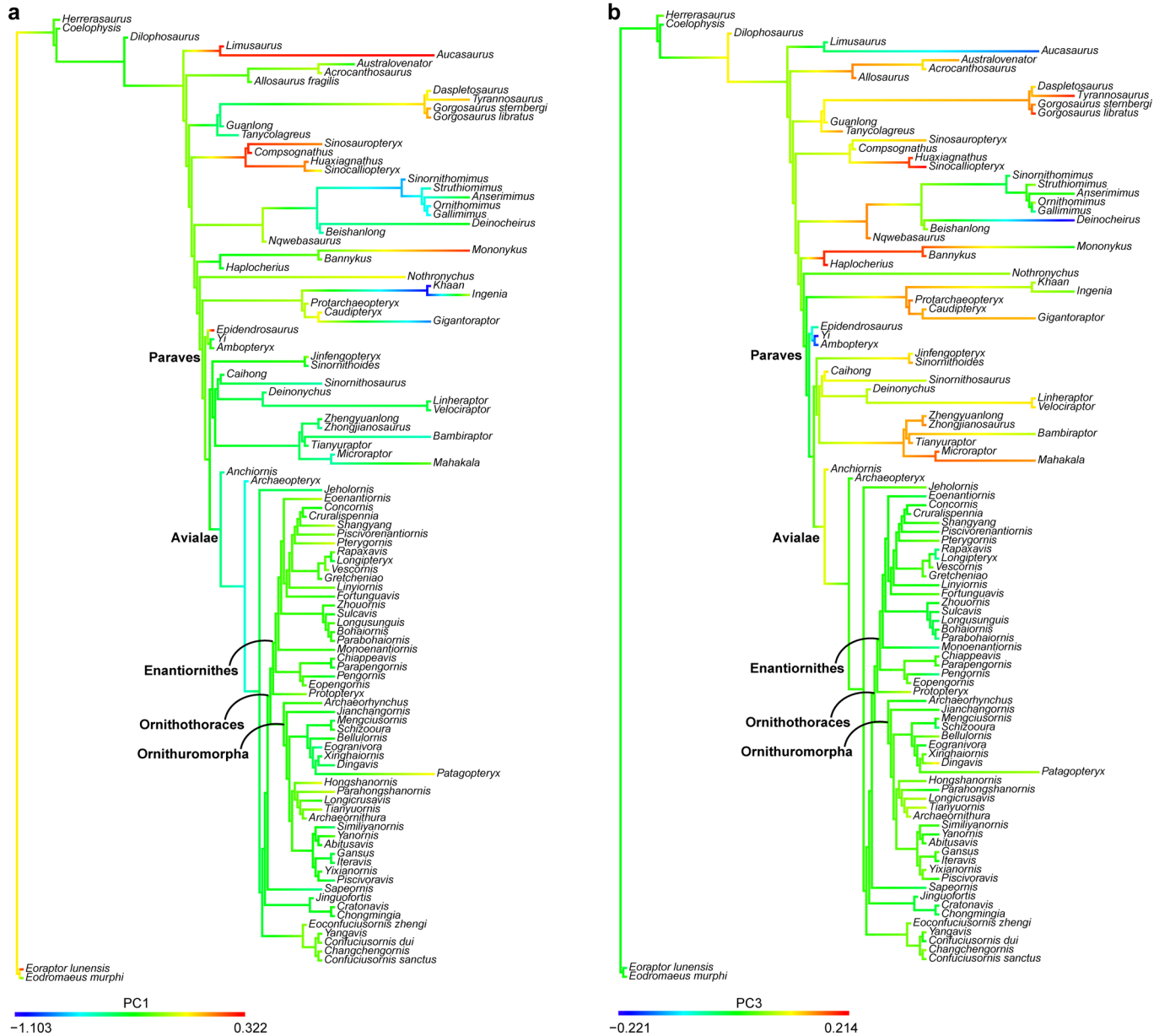

Extended Data Fig. 1 | Evolutionary changes of all appendicular elements across Mesozoic theropod phylogeny. The first and third principal components (PCs) derived from pPCA of all limbs are mapped on the time-calibrated tree. **a**, PC1 (=70.03% variances). **b**, PC3 (=6.7% variances).

https://doi.org/10.1038/s41559-023-02091-z

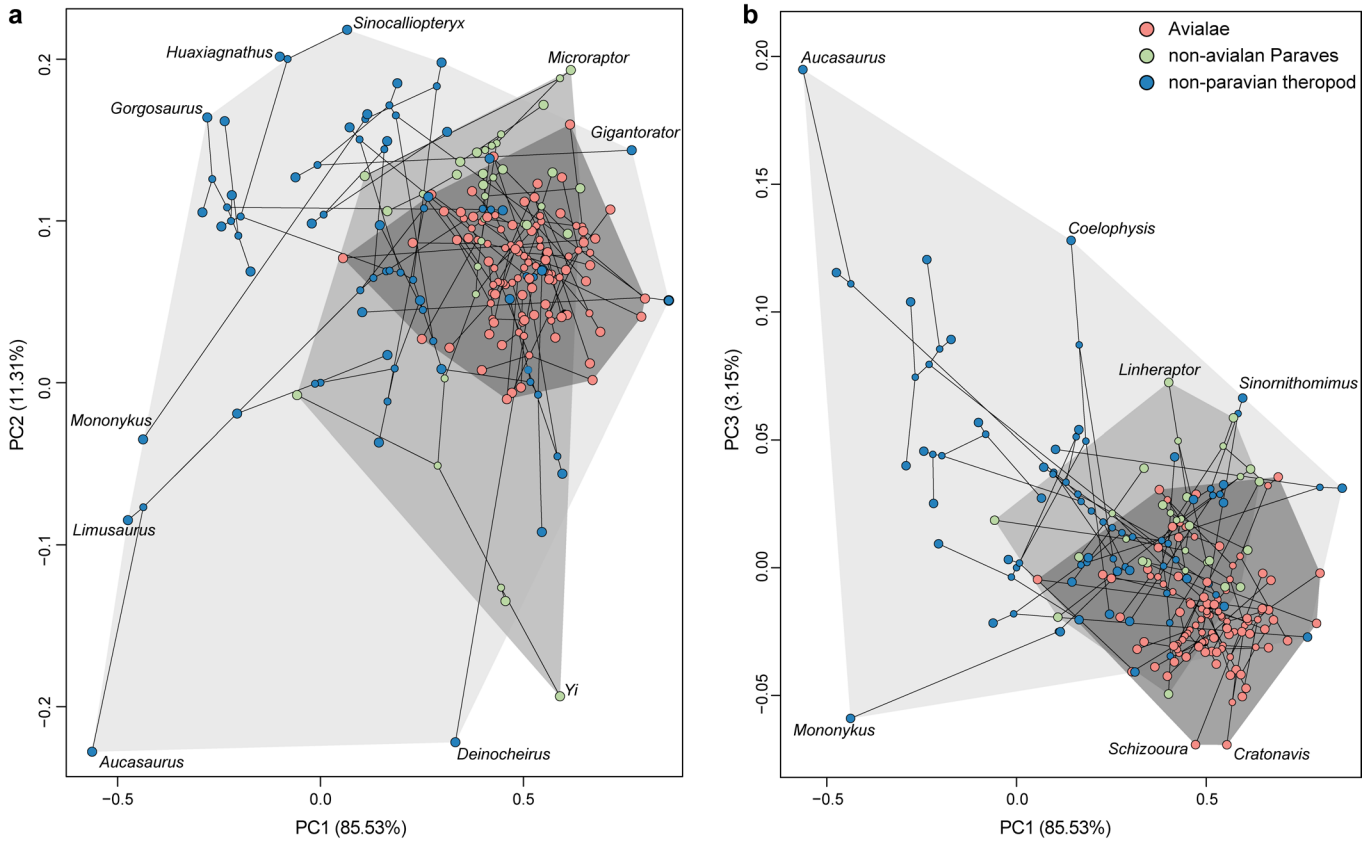

Extended Data Fig. 2 | Phylomorphospace of forelimb morphological disparity of Mesozoic theropods. The first three principal components (PCs) derived from pPCA of forelimb are used. **a**, Binary plot of PCs 1 and 2. **b**, Binary plot of PCs 1 and 3.

https://doi.org/10.1038/s41559-023-02091-z

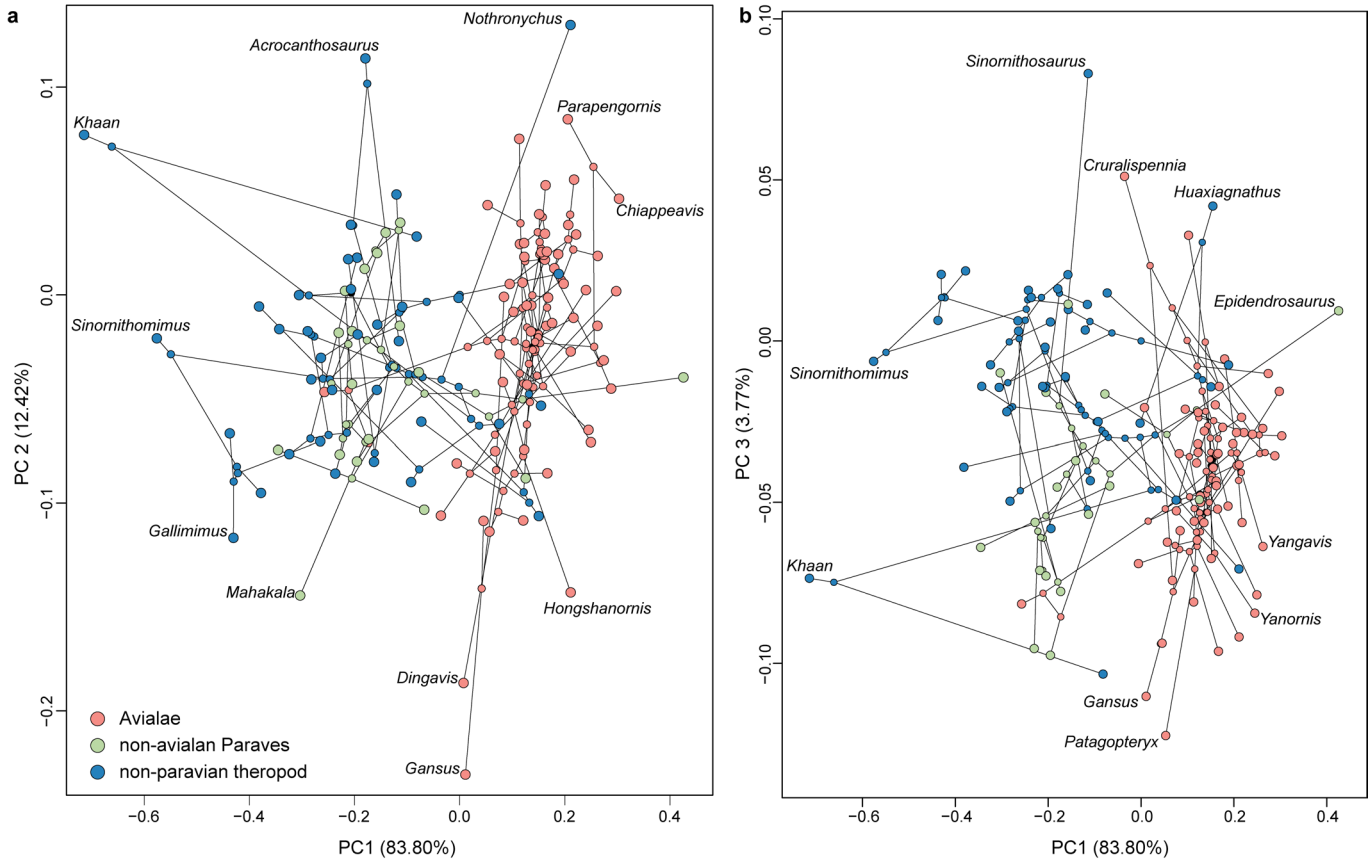

Extended Data Fig. 3 | Phylomorphospace of hindlimb morphological disparity of Mesozoic theropods. The first three principal components (PCs) derived from pPCA of hindlimb are used. **a**, Binary plot of PCs 1 and 2. **b**, Binary plot of PCs 1 and 3.

https://doi.org/10.1038/s41559-023-02091-z

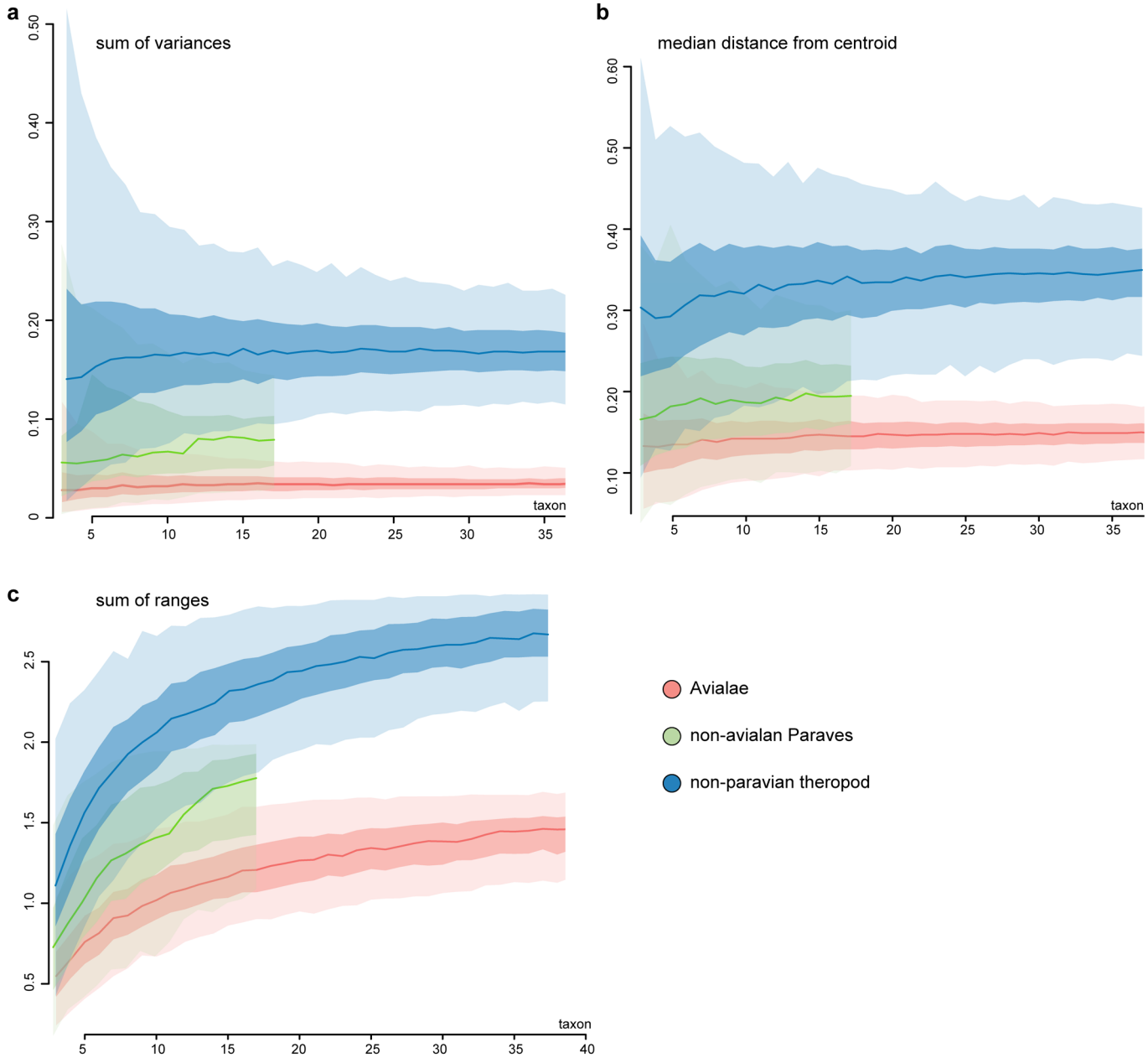

Extended Data Fig. 4 | Rarefaction of disparity curves of Mesozoic theropods showing that the results are not strongly affected by sampling bias. Morphological disparity is quantified using three metrices: **a**, sum of variances; **b**, median distance from centroid; **c**, and sum of ranges. The dark and light surfaces indicate the 50% and 95% confidence intervals, respectively.

https://doi.org/10.1038/s41559-023-02091-z

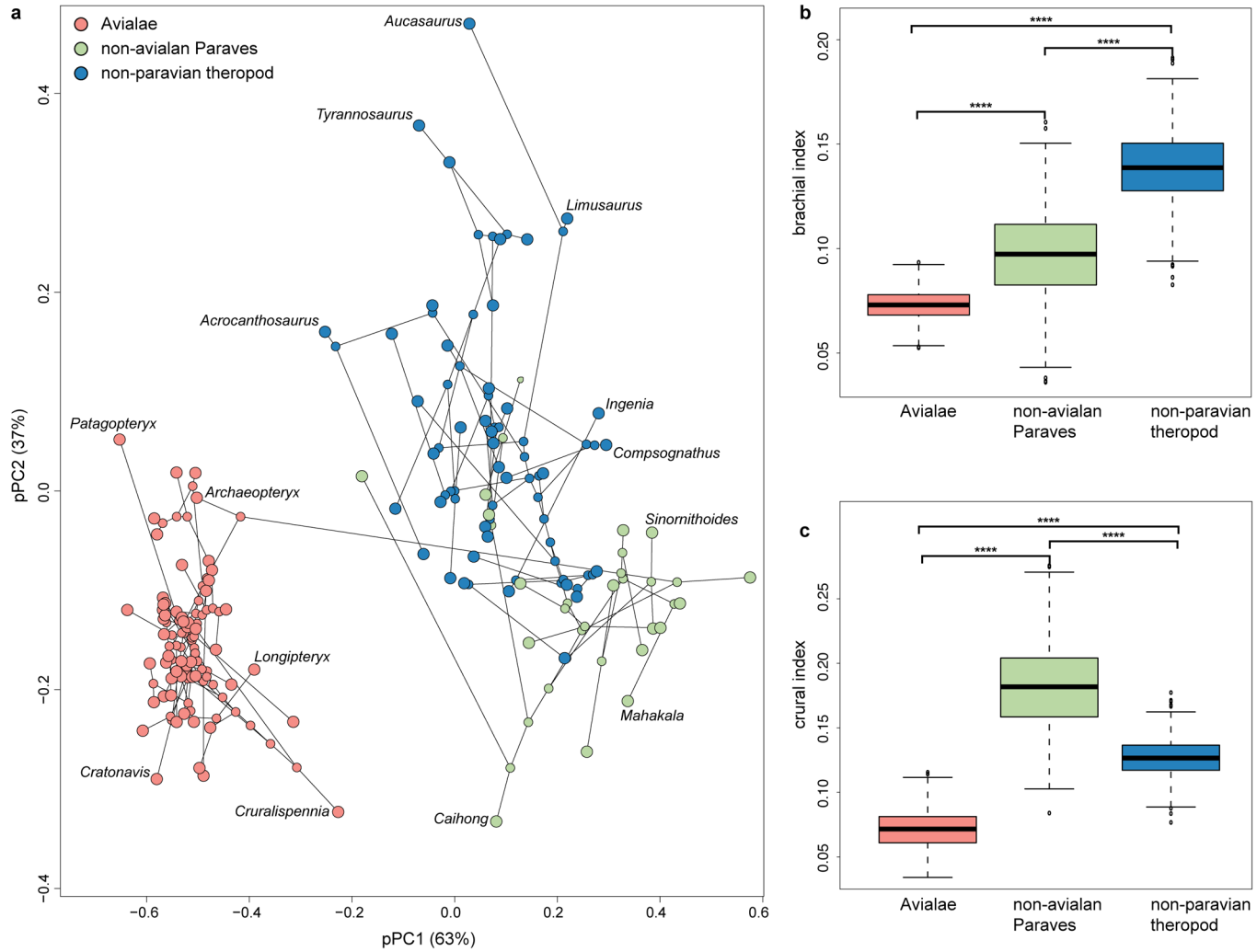

Extended Data Fig. 5 | Evolutionary changes of brachial (BI) and crural (CI) indices across Mesozoic theropod phylogeny. a, Phylomorphospace of BI and crural CI indices with phylogeny accounted. **b, c**, Comparison of disparity among three subgroups using standard deviations of BI (**b**) and CI (**c**), respectively (The boxes represent the median, the first and the third quartile of the morphological disparity; $n = 109$ species). Morphological disparity was compared using Welch's t-test for statistical significance (****two-sided p-value threshold <0.05).

https://doi.org/10.1038/s41559-023-02091-z

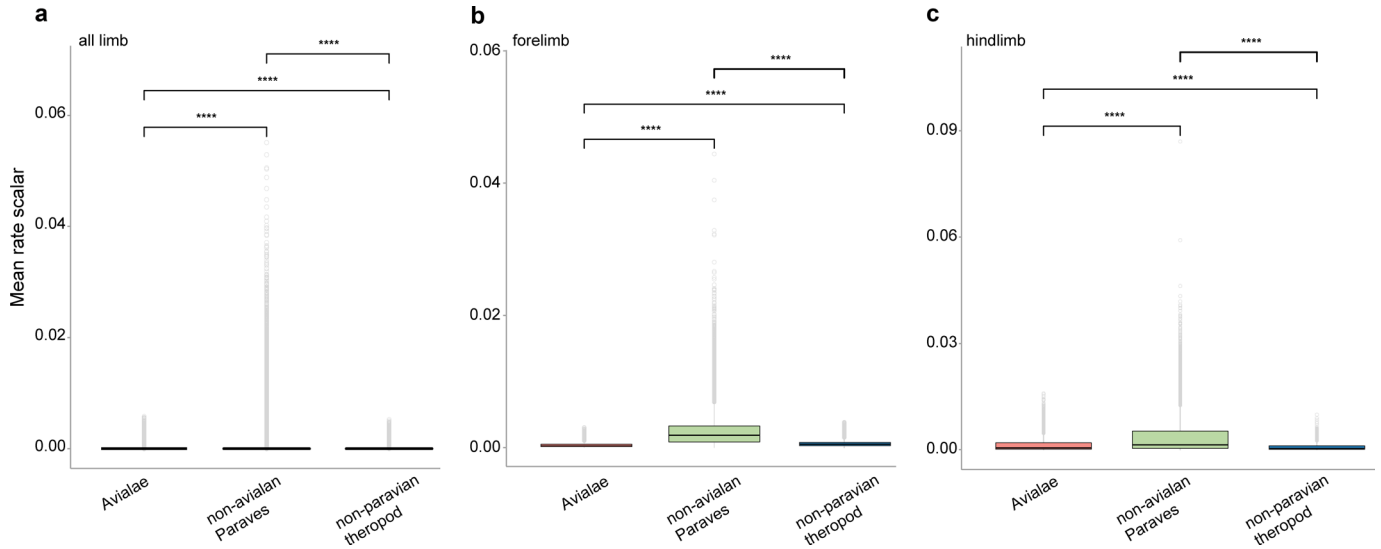

Extended Data Fig. 6 | Comparison of evolutionary rate of subgroups of Mesozoic theropods. Evolutionary rates are significantly different in all pairwise comparisons. The mean rate scalar is the mean of the rate scalars calculated in the post-burn-in posterior distribution under the variable rate evolutionary model (The boxes represent the median, the first and the third quartile of the mean rate scalar; $n = 109$ species). **a**, All appendicular elements. **b**, Forelimb. **c**, Hindlimb. Evolutionary rate among subgroups were compared using a nonparametric *t*-test for statistical significance (****: $p < 0.00005$).

https://doi.org/10.1038/s41559-023-02091-z

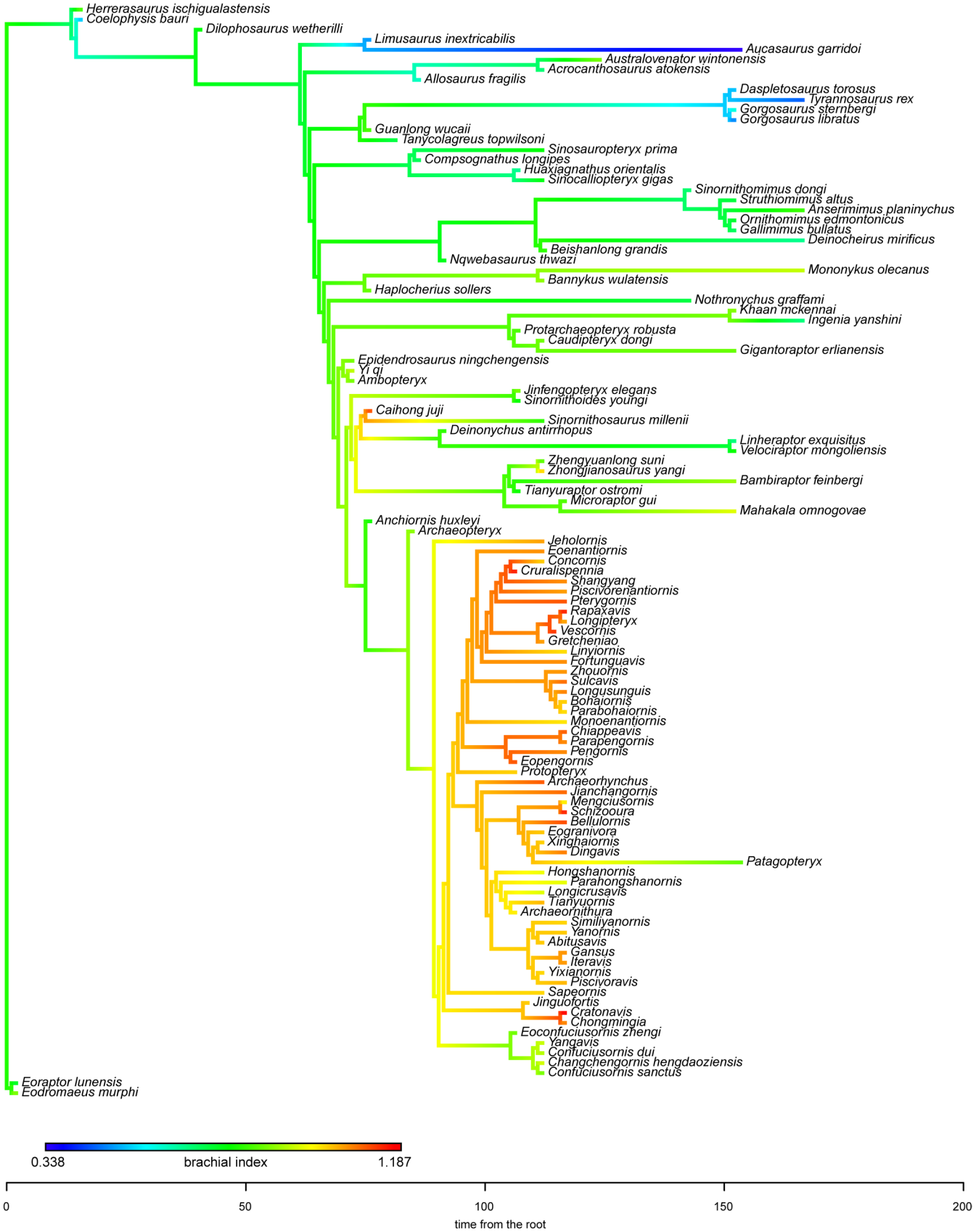

Extended Data Fig. 7 | Evolutionary changes of brachial index across time-calibrated Mesozoic theropod tree.

https://doi.org/10.1038/s41559-023-02091-z

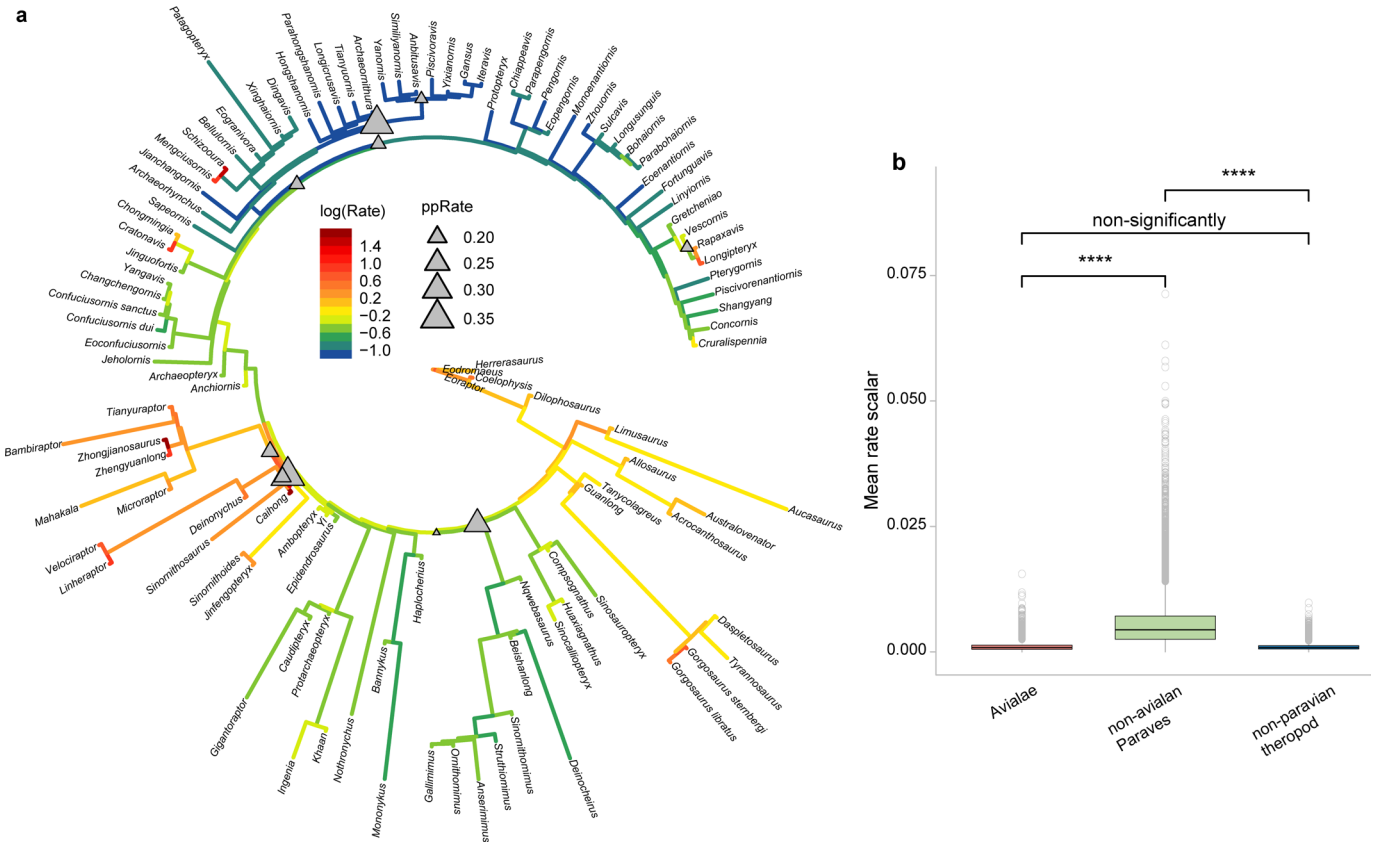

Extended Data Fig. 8 | Evolutionary changes of brachial index across Mesozoic theropod phylogeny. a, Branch specific evolutionary rates and rate shifts (Branch specific evolutionary rates are denoted by the color gradients. Posterior probabilities of rate shifts are indicated by the relative size of the grey triangles). **b**, Comparison of evolutionary rate of brachial index among subgroups (The boxes represent the median, the first and the third quartile of the mean rate scalar; $n = 109$ species). Evolutionary rates are significantly different in all pairwise comparisons except between Avialae and non-paravian theropods.

https://doi.org/10.1038/s41559-023-02091-z

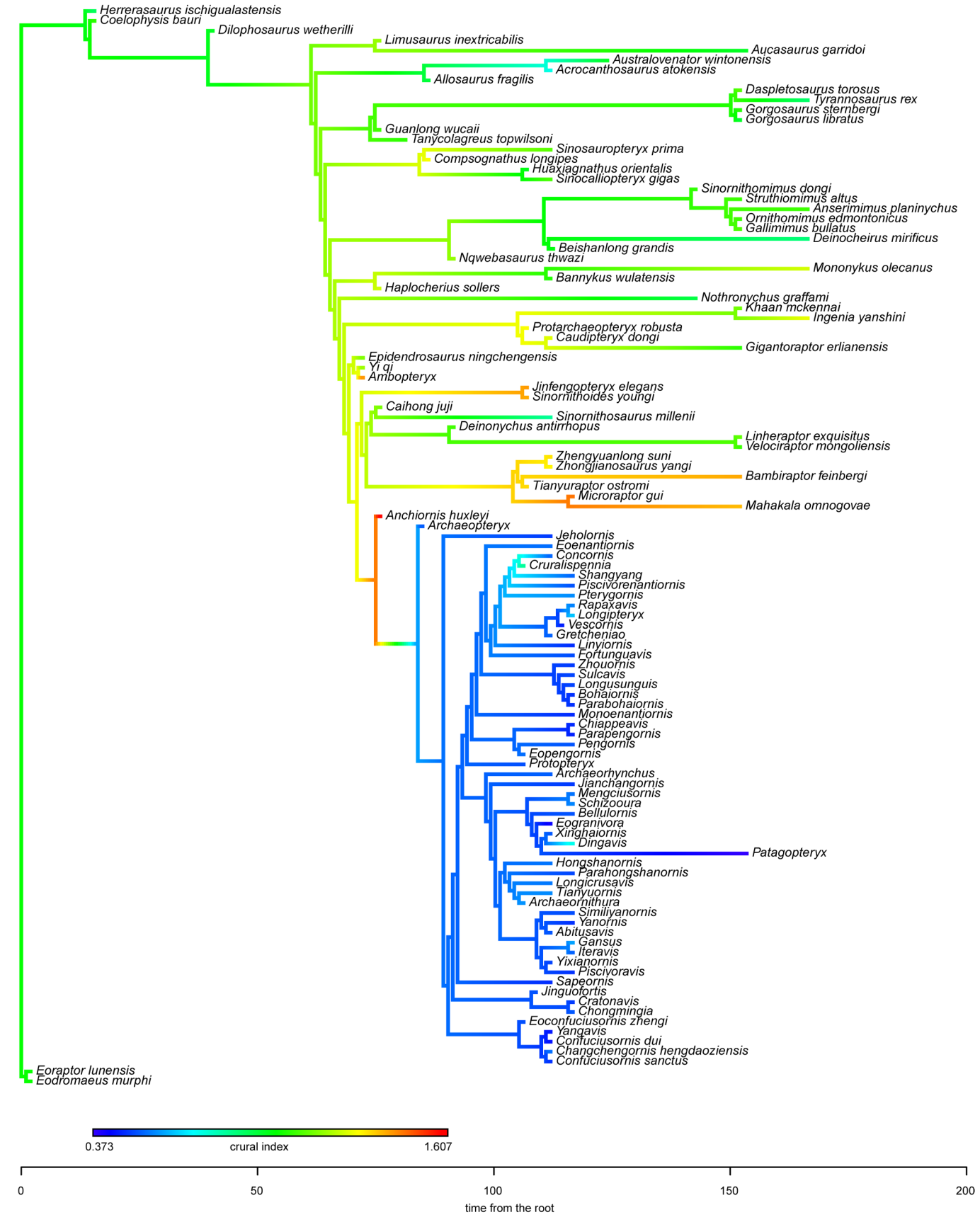

Extended Data Fig. 9 | Evolutionary changes of crural index across time-calibrated Mesozoic theropod tree.

https://doi.org/10.1038/s41559-023-02091-z

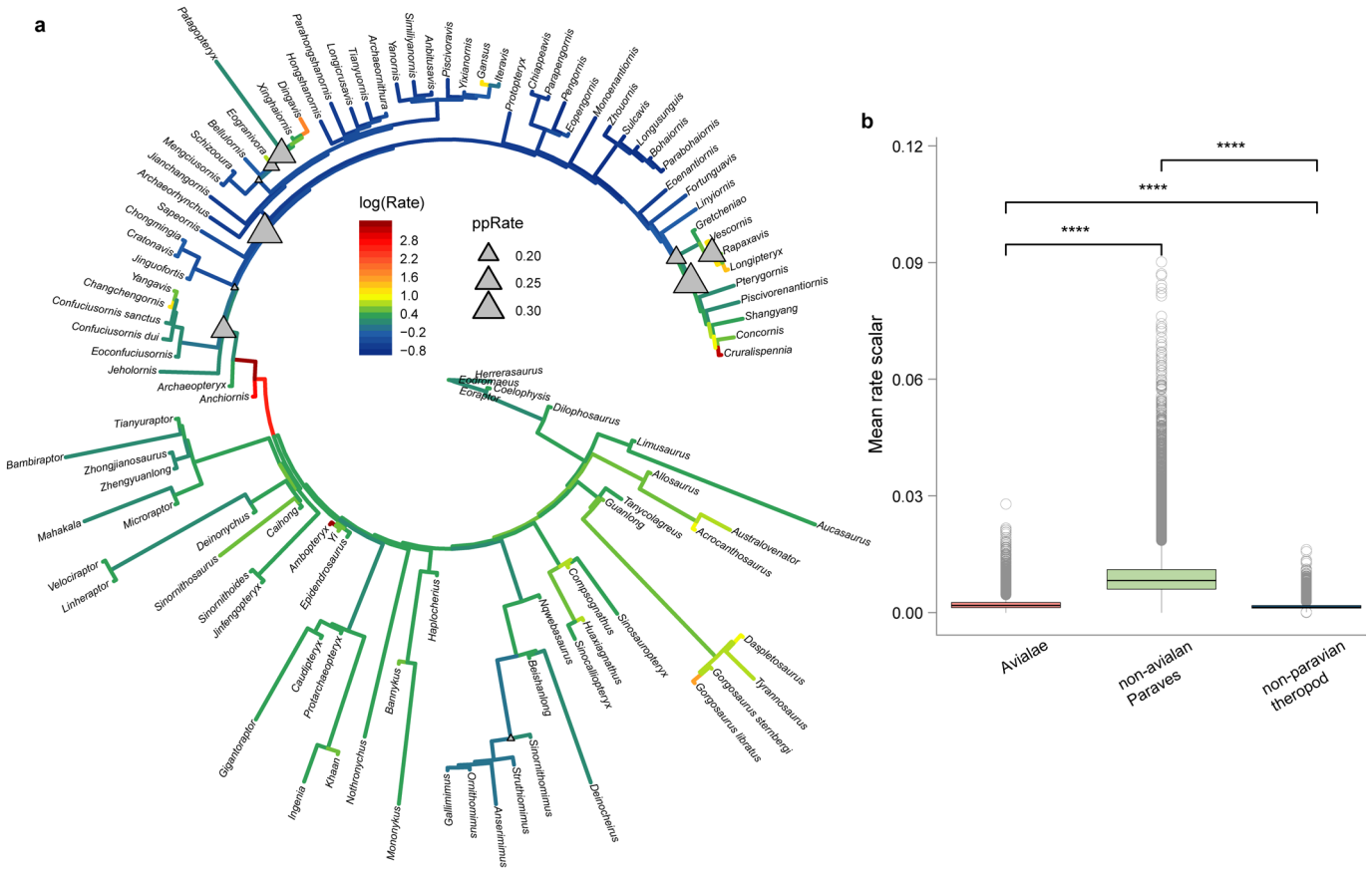

Extended Data Fig. 10 | Evolutionary changes of crural index across Mesozoic theropod phylogeny. a, Branch specific evolutionary rates and rate shifts (Branch specific evolutionary rates are denoted by the color gradients. Posterior probabilities of rate shifts are indicated by the relative size of the grey triangles). **b**, Comparison of evolutionary rate of brachial index among subgroups (The boxes represent the median, the first and the third quartile of the mean rate scalar; $n = 109$ species). Evolutionary rates are significantly different in all pairwise comparisons.

nature portfolio

Corresponding author(s): MIN WANG

Last updated by author(s): 2023-4-28

Reporting Summary

Nature Portfolio wishes to improve the reproducibility of the work that we publish. This form provides structure for consistency and transparency in reporting. For further information on Nature Portfolio policies, see our Editorial Policies and the Editorial Policy Checklist.

Statistics

For all statistical analyses, confirm that the following items are present in the figure legend, table legend, main text, or Methods section.

n/a	Confirmed	
☐	☒	The exact sample size (*n*) for each experimental group/condition, given as a discrete number and unit of measurement
☐	☒	A statement on whether measurements were taken from distinct samples or whether the same sample was measured repeatedly
☐	☒	The statistical test(s) used AND whether they are one- or two-sided *Only common tests should be described solely by name; describe more complex techniques in the Methods section.*
☒	☐	A description of all covariates tested
☒	☐	A description of any assumptions or corrections, such as tests of normality and adjustment for multiple comparisons
☒	☐	A full description of the statistical parameters including central tendency (e.g. means) or other basic estimates (e.g. regression coefficient) AND variation (e.g. standard deviation) or associated estimates of uncertainty (e.g. confidence intervals)
☒	☐	For null hypothesis testing, the test statistic (e.g. *F*, *t*, *r*) with confidence intervals, effect sizes, degrees of freedom and *P* value noted *Give P values as exact values whenever suitable.*
☐	☒	For Bayesian analysis, information on the choice of priors and Markov chain Monte Carlo settings
☒	☐	For hierarchical and complex designs, identification of the appropriate level for tests and full reporting of outcomes
☒	☐	Estimates of effect sizes (e.g. Cohen's *d*, Pearson's *r*), indicating how they were calculated

Our web collection on statistics for biologists contains articles on many of the points above.

Software and code

Policy information about availability of computer code

Data collection	The length measurements—humerus, ulna/radius, metacarpal II (carpometacarpus for avialans), femur, tibia (tibiotarsus for avialans), and metatarsal III (tarsometatarsus for avialans) of Mesozoic theropodS—were obtained by direct measurement in combined with published source data
Data analysis	Analyses of morphological disparity were conducted in R using relevant functions including phyl.resid, phyl.pca, adonis, gelman.diag and effectiveSize. Evolutionary rate analyses were performed using the BayesTraitsV4 (http://www.evolution.rdg.ac.uk).

For manuscripts utilizing custom algorithms or software that are central to the research but not yet described in published literature, software must be made available to editors and reviewers. We strongly encourage code deposition in a community repository (e.g. GitHub). See the Nature Portfolio guidelines for submitting code & software for further information.

Data

Policy information about availability of data

All manuscripts must include a data availability statement. This statement should provide the following information, where applicable:

- Accession codes, unique identifiers, or web links for publicly available datasets
- A description of any restrictions on data availability
- For clinical datasets or third party data, please ensure that the statement adheres to our policy

Provide your data availability statement here.

Research involving human participants, their data, or biological material

Policy information about studies with human participants or human data. See also policy information about sex, gender (identity/presentation), and sexual orientation and race, ethnicity and racism.

Reporting on sex and gender	Not applicable
Reporting on race, ethnicity, or other socially relevant groupings	Not applicable
Population characteristics	Not applicable
Recruitment	Not applicable
Ethics oversight	Not applicable

Note that full information on the approval of the study protocol must also be provided in the manuscript.

Field-specific reporting

Please select the one below that is the best fit for your research. If you are not sure, read the appropriate sections before making your selection.

☐ Life sciences ☐ Behavioural & social sciences ☒ Ecological, evolutionary & environmental sciences

For a reference copy of the document with all sections, see nature.com/documents/nr-reporting-summary-flat.pdf

Ecological, evolutionary & environmental sciences study design

All studies must disclose on these points even when the disclosure is negative.

Study description	This study analyses the morphological disparity and evolutionary rate of limb bone size during the theropod-birds transition.
Research sample	To investigate changes of body shape close to the origin of the Avialae, we complied linear measurements of limb bones across the whole spectrum of Mesozoic theropod phylogeny, including early diverging avialans. The length measurements—humerus, ulna/radius, metacarpal II (carpometacarpus for avialans), femur, tibia (tibiotarsus for avialans), and metatarsal III (tarsometatarsus for avialans)—were obtained by direct measurement in combined with published source data.
Sampling strategy	We compiled a large sample of Mesozoic theropod specimens that completely preserve the six appendicular limb elements.
Data collection	Linear measurements of limb bones across the whole spectrum of Mesozoic theropod phylogeny were obtained by direct measurement in combined with published source data by the corresponding author Min Wang.
Timing and spatial scale	The fossil samples span the whole spectrum of Mesozoic theropod phylogeny.
Data exclusions	We omitted specimens that do not preserve complete length for all six limb bones, given the controversy regarding scaling relationships of limb size.
Reproducibility	The R code is accessible at Figshare as well as OSF (https://osf.io/8n3wt/?view_only=753148d6a15f478e8fa027890b6b9bde), and can be used to reproduce the results presented in this manuscript.
Randomization	Not applicable
Blinding	Not applicable

Did the study involve field work? ☐ Yes ☒ No

Reporting for specific materials, systems and methods

We require information from authors about some types of materials, experimental systems and methods used in many studies. Here, indicate whether each material, system or method listed is relevant to your study. If you are not sure if a list item applies to your research, read the appropriate section before selecting a response.

Materials & experimental systems

n/a	Involved in the study
☒	☐ Antibodies
☒	☐ Eukaryotic cell lines
☐	☒ Palaeontology and archaeology
☒	☐ Animals and other organisms
☒	☐ Clinical data
☒	☐ Dual use research of concern
☒	☐ Plants

Methods

n/a	Involved in the study
☒	☐ ChIP-seq
☒	☐ Flow cytometry
☒	☐ MRI-based neuroimaging

Palaeontology and Archaeology

Specimen provenance	Linear measurements of limb bones across the whole spectrum of Mesozoic theropod phylogeny were obtained by direct measurement in combined with published source data. The raw data is available in the Supplementary information.
Specimen deposition	The R code, raw data, and results derived from the phylogeny scaled using the “equal” method are available at Figshare as well as OSF (https://osf.io/8n3wt/?view_only=753148d6a15f478e8fa027890b6b9bde).
Dating methods	Not applicable

☒ Tick this box to confirm that the raw and calibrated dates are available in the paper or in Supplementary Information.

Ethics oversight	Institute of Vertebrate Paleontology and Paleoanthropology has approved the study protocol

Note that full information on the approval of the study protocol must also be provided in the manuscript.